A PML Using a Convolutional Curl Operator and a Numerical Reflection Coefficient for General Linear Media

Michael W. Chevalier and Umran S. Inan, *Senior Member, IEEE*

***Abstract*—A general time domain representation of the Chew and Weedon [1994] stretched coordinate perfectly matched layer (PML) absorbing boundary condition is described. This new approach mathematically operates on the spatial field derivatives and allows the PML update equations to be trivially derived from any set of general linear medium update equations. A method for calculating the frequency dependent reflection coefficient for this form of the PML is derived for general linear media. Two and three dimensional numerical test results, which validate the calculation of the reflection coefficient, are presented. The range of numerical tests include the PML matching of free space, a magnetoplasma, and a free space waveguide. Improving the reflection coefficient is examined.**

***Index Terms*—Perfectly matched layer (PML), recursive convolution, reflection coefficient.**

I. Introduction

THE introductions of the perfectly matched layer (PML) by Berenger [1] and Chew and Weedon [2] has revolutionized the state-of-the-art in the use of absorbing boundary conditions for the finite-difference time-domain (FDTD) technique as well as for other methods of numerical electromagnetic modeling. Although both approaches were originally derived to match lossless dielectric media, there has since been efforts by other researchers to advance the PML to match general linear media, including linear anisotropic media. These advancements include Gedney's approach [8], the uniaxial PML, which is Maxwellian and which does not require the field splitting technique employed by [1] and [2], and which has been derived to match linear isotropic media. Fang [4] describes the generalized perfectly matched layer which is an extension of [1] to match lossy isotropic media, using the field splitting technique. Finally, a recent paper by Texierra [5] recognizes that [1] and [2] are applicable to general linear media, including anisotropic media, while continuing to employ the field splitting technique. In the present paper we build upon and extend this past work starting from [5].

Section III represents the contents of [6], a presentation given at the URSI conference in Boulder, CO, in 1999. We reference Roden and Gedney [7], which involved the CPML (convolutional PML), a method similar to that presented here (both apply the recursive convolution technique) and whose work was also carried out during an overlapping time period. In Section IV we mathematically compare the CPML with the PML presented in this paper to show that the latter has a more general form. Gedney *et al.* [8] have also applied the CPML technique to establish an unconditionally stable alternating-direction implicit FDTD (ADI-FDTD) method. Since the arrival of the CPML, there have been other unsplit time domain formulations developed. Ramadan [9] used the unsplit formulation to derive a time domain formulation using DSP techniques.

A method for calculating the numerical reflection coefficient for our form of the PML is developed in the current paper. Numerical reflection coefficient calculations have been done in previous papers. These include Chew [10] and Fang [11] and Berenger [12] who have all developed reflection calculations from a multilayered split field PML. Berenger [13] develops and investigates the numerical reflection coefficients for particular cases of nonlossy isotropic media for various PMLs [including split field, unsplit field, and complex frequency shifted PML (CFS-PML)]. Berenger also [14] investigates optimizing numerical reflection coefficients for evanescent and propagating waves for the CFS-PML in waveguides. We build upon this past work by deriving the numerical reflection coefficient for our form of the PML for general linear media, including anisotropic media. We also demonstrate the application of optimization techniques to improve the numerical reflection coefficient of this PML for a range of mediums including free space, waveguides, and magnetized plasma.

II. General Frequency Domain PML Equations

We express the Chew and Weedon equations in a different form than that derived in [2], which is more easily adapted to the new time domain technique for the PML. We start with the general three-dimensional (3-D) PML equations

$$\nabla_{\mathrm{PML}} = \frac{1}{1+g_x(j\omega)}\frac{\partial}{\partial x}\hat{a}_x + \frac{1}{1+g_y(j\omega)}\frac{\partial}{\partial y}\hat{a}_y + \frac{1}{1+g_z(j\omega)}\frac{\partial}{\partial z}\hat{a}_z \tag{1a}$$

$$\nabla_{\mathrm{PML}} \times \vec{H} = j\omega\varepsilon\vec{E} + \vec{J} \tag{1b}$$

$$\nabla_{\mathrm{PML}} \times \vec{E} = -j\omega\mu_0\vec{H} \tag{1c}$$

$$\vec{J} = \sigma\vec{E} \tag{1d}$$

$$\text{solution form}: e^{-jk[x\sin(\theta)\cos(\phi)+y\sin(\theta)\sin(\phi)+z\cos(\theta)]} \times e^{-jk[g_x(j\omega)x\sin(\theta)\cos(\phi)+g_y(j\omega)y\sin(\theta)\sin(\phi)+g_z(j\omega)z\cos(\theta)]}$$

Manuscript received January 14, 2003; revised September 1, 2003. This work was supported in part by a NASA GSRP Fellowship and in part by the NSF under Grant ATM-9819936-002.

The authors are with the Space, Telecommunications, and Radioscience Laboratory of the Department of Electrical Engineering, Stanford University, Stanford, CA 94305 USA (e-mail: mwc@nova.stanford.edu; inan@nova.stanford.edu).

Digital Object Identifier 10.1109/TAP.2004.831318

where ε is isotropic permittivity, σ is the conductivity and can be an anisotropic tensor, and k is the wavenumber, which can be a function of both ω, θ and ϕ. We define ω as the radial frequency, θ as the angle with respect to the z axis, and ϕ as the azimuthal angle in the xy plane with respect to the x axis. The form of the solution can be verified by direct substitution into the equations. Maxwell's equations and their traditional plane wave solution can be obtained from (1) by setting $g_x(j\omega) = g_y(j\omega) = g_z(j\omega) = 0$. The plane wave solution of the PML is the same as that of Maxwell equations except that it is multiplied by a second exponential function, which represents the adjustable dissipation of the PML and which can in general be a complex and frequency-dependent function. The various impedance relationships inherent in (1a), e.g., E_x/H_y, can easily be shown to be identical to those obtained from Maxwell's equations. We can rewrite the $\nabla_{\rm PML}$ operator as

$$\nabla_{\rm PML} = \left[\frac{\partial}{\partial x} - \frac{g_x(j\omega)}{1+g_x(j\omega)}\frac{\partial}{\partial x}\right]\hat{a}_x + \left[\frac{\partial}{\partial y} - \frac{g_y(j\omega)}{1+g_y(j\omega)}\frac{\partial}{\partial y}\right]\hat{a}_y + \left[\frac{\partial}{\partial z} - \frac{g_z(j\omega)}{1+g_z(j\omega)}\frac{\partial}{\partial z}\right]\hat{a}_z. \quad (2)$$

This form allows the PML to be implemented without the need for the field splitting technique.

III. First-Order Time-Dependent Curl Operator PML Equations

If we let $g_x(j\omega) = \alpha_x/j\omega$, $g_y(j\omega) = \alpha_y/j\omega$, and $g_z(j\omega) = \alpha_z/j\omega$, where α_x, α_y, and α_z are positive real constants, the time domain $\nabla_{\rm PML}$ operator becomes

$$\nabla_{\rm PML} = \left[\frac{\partial}{\partial x} - u(t)\alpha_x e^{-\alpha_x t} * \frac{\partial}{\partial x}\right]\hat{a}_x + \left[\frac{\partial}{\partial y} - u(t)\alpha_y e^{-\alpha_y t} * \frac{\partial}{\partial y}\right]\hat{a}_y + \left[\frac{\partial}{\partial z} - u(t)\alpha_z e^{-\alpha_z t} * \frac{\partial}{\partial z}\right]\hat{a}_z \quad (3)$$

where "$*$" represents convolution and $u(t)$ is the unit step function. This form of the PML has a temporal/spatial operation which involves a convolution between a decaying exponential and the function that the spatial derivative operates on. It is hereafter referred to as the first-order convolutional curl operation PML (CCO-PML) or sometimes just as CCO-PML. Mathematically, the first-order CCO-PML yields the same solutions as the final time domain representations of Berenger [1] and Chew and Weedon [2]. In this form, unlike prior forms used in [1] and [2], the first-order CCO-PML trivially matches any general linear medium, including anisotropic media. Invoking linearity we can arrange the CCO-PML equations derived from (1a) into

$$[\nabla_{\rm PML} - \nabla] \times \vec{H} + \nabla \times \vec{H} = \frac{\partial \varepsilon * \vec{E}}{\partial t} + \vec{J} \quad (4a)$$

$$[\nabla_{\rm PML} - \nabla] \times \vec{E} + \nabla \times \vec{E} = -\mu_0 \frac{\partial \vec{H}}{\partial t} \quad (4b)$$

where

$$\begin{aligned}[\nabla_{\rm PML} - \nabla] \times \vec{H} &= -\left[u(t)\alpha_y e^{-\alpha_y t} * \frac{\partial H_z}{\partial y} - u(t)\alpha_z e^{-\alpha_z t} * \frac{\partial H_y}{\partial z}\right]\hat{a}_x \\ &\quad -\left[u(t)\alpha_z e^{-\alpha_z t} * \frac{\partial H_x}{\partial z} - u(t)\alpha_x e^{-\alpha_x t} * \frac{\partial H_z}{\partial x}\right]\hat{a}_y \\ &\quad -\left[u(t)\alpha_x e^{-\alpha_x t} * \frac{\partial H_y}{\partial x} - u(t)\alpha_y e^{-\alpha_y t} * \frac{\partial H_x}{\partial y}\right]\hat{a}_z \quad (5)\end{aligned}$$

and the corresponding curl of the electric field, i.e., $[\nabla_{\rm PML} - \nabla] \times \vec{E}$, has the same form as above and can be obtained simply by replacing $\vec{H}$'s with $\vec{E}$'s. The Maxwellian update equations and the CCO-PML update equations are identical except for the extra convolution terms included in the CCO-PML update equations. The convolutions can be efficiently calculated using the piecewise linear recursive convolution technique of Kelley and Luebbers [15]. The memory requirements are larger for the CCO-PML update equations relative to their Maxwellian counterparts, since at the location of each field component up to two convolution sums must be stored. Nevertheless, detailed analysis indicates that the memory requirements are similar to those for the free space PML derived in [1]. It should be noted the number of extra variables needed to implement the first-order CCO-PML does not depend on the complexity of the medium.

IV. General Nth-Order CCO-PML

For complicated dispersive media such as magnetized plasmas the optimized first-order CCO-PML for a given thickness T may not achieve the desired reflection coefficient over the frequency range of interest. We may, therefore, try to improve the performance of the CCO-PML by including more convolutional terms. We can assume

$$\frac{1}{1+g_x(j\omega)} = 1 - \sum_{n=1}^{N} \frac{b_{xn}\alpha_{xn}}{j\omega + \alpha_{xn}} \quad (6)$$

where $1/(1+g_y(j\omega))$ and $1/(1+g_z(j\omega))$ have the same form also. In which case the frequency domain $\nabla_{\rm PML}$ operator becomes

$$\nabla_{\rm PML} = \left[\frac{\partial}{\partial x} - \left(\sum_{n=1}^{N} \frac{b_{xn}\alpha_{xn}}{j\omega + \alpha_{xn}}\right)\frac{\partial}{\partial x}\right]\hat{a}_x + \left[\frac{\partial}{\partial y} - \left(\sum_{n=1}^{N} \frac{b_{yn}\alpha_{yn}}{j\omega + \alpha_{yn}}\right)\frac{\partial}{\partial y}\right]\hat{a}_y + \left[\frac{\partial}{\partial z} - \left(\sum_{n=1}^{N} \frac{b_{zn}\alpha_{zn}}{j\omega + \alpha_{zn}}\right)\frac{\partial}{\partial z}\right]\hat{a}_z. \quad (7)$$

It is easy to show that with this higher order $\nabla_{\rm PML}$ operator the PML character of the equation is still mathematically preserved. The time domain $[\nabla_{\rm PML} - \nabla] \times \vec{H}$ becomes

$$\begin{aligned}[\nabla_{\rm PML}-\nabla]\times\vec{H} &= -\left\{Re\left\{\sum_{n=1}^{N} u(t)b_{yn}\alpha_{yn}e^{-\alpha_{yn}t}\right\}*\frac{\partial H_z}{\partial y}\right. \\ &\quad \left. -Re\left\{\sum_{n=1}^{N} u(t)b_{zn}\alpha_{zn}e^{-\alpha_{zn}t}\right\}*\frac{\partial H_y}{\partial z}\right\}\hat{a}_x \\ &\quad -\left\{Re\left\{\sum_{n=1}^{N} u(t)b_{zn}\alpha_{zn}e^{-\alpha_{zn}t}\right\}*\frac{\partial H_x}{\partial z}\right. \\ &\quad \left. -Re\left\{\sum_{n=1}^{N} u(t)b_{xn}\alpha_{xn}e^{-\alpha_{xn}t}\right\}*\frac{\partial H_z}{\partial x}\right\}\hat{a}_y \\ &\quad -\left\{Re\left\{\sum_{n=1}^{N} u(t)b_{xn}\alpha_{xn}e^{-\alpha_{xn}t}\right\}*\frac{\partial H_y}{\partial x}\right. \\ &\quad \left. -Re\left\{\sum_{n=1}^{N} u(t)b_{yn}\alpha_{yn}e^{-\alpha_{yn}t}\right\}*\frac{\partial H_x}{\partial y}\right\}\hat{a}_z \quad (8)\end{aligned}$$

where $b_{xn}(i)$ and $\alpha_{xn}(i)$, also known as the CCO-PML coefficients, can be complex (note: For complex coefficients we take the real part of the convolution, e.g., $Re\{u(t)b_{x1}\alpha_{x1}e^{-\alpha_{x1}t}\} * (\partial H_z/\partial x)$, because the functions that are convolved with the fields must be real. An equivalent statement to $Re\{u(t)b_{x1}\alpha_{x1}e^{-\alpha_{x1}t}\} * (\partial H_z/\partial x)$ is $(1/2)\{u(t)b_{x1}\alpha_{x1}e^{-\alpha_{x1}t} + u(t)b^*_{x1}\alpha^*_{x1}e^{-\alpha^*_{x1}t}\}*(\partial H_z/\partial x)$ which is used in the next section of this paper. Also, note that complex convolutions require twice as much memory. If memory is an issue real valued coefficients should be used. Note that $[\nabla_{\rm PML} - \nabla] \times \vec{E}$ has the same form as above; obtained by replacing the $\vec{H}$'s with $\vec{E}$'s. The equations for the Nth order CCO-PML are no more difficult to solve than those for the first-order CCO-PML, except that N times as many convolutions are involved all of which can be readily computed with the piecewise linear recursive convolution technique of [15]. The question arises: Why not double the thickness of the PML instead of including extra convolutional terms? By doubling the thickness we increase, within the PML, the computational time and the number of variables by a factor of 2. Most of the PML has loss in only one direction, except at the edges and the corners. Assuming this and a free space grid, if we increase the number of convolutional terms to, say $N = 2$, it can easily be shown that we increase, within the PML, the computational time and the number of extra update variables by a factor of 1.4. For $N = 3$, this factor would be 1.8. The saving would be even greater for grids containing more complex materials where prior values of the fields need to be saved, such as Lorentz or Debye materials.

To demonstrate the generality of the scheme we derive the standard form given in [7] from an order, $N = 2$, CCO-PML. We direct our analysis at the $(\partial H_z/\partial x) - Re[\sum_{n=1}^{N} u(t)b_{xn}\alpha_{xn}e^{-\alpha_{xn}t}] * (\partial H_z/\partial x)$ term whose results are easily generalized. Knowing that $(\partial H_z/\partial x) = \delta(t) * (\partial H_z/\partial x)$ and substituting this into the term we get $[\delta(t) - u(t)b_{x1}\alpha_{x1}e^{-\alpha_{x1}t} - u(t)b_{x2}\alpha_{x2}e^{-\alpha_{x2}t}]*(\partial H_z/\partial x)$.

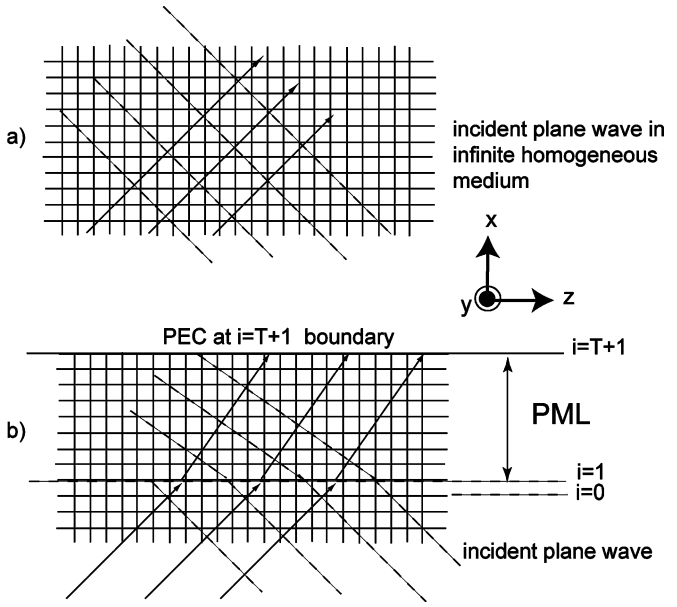

Fig. 1. Illustration of plane waves traveling within an FDTD grid. (a) Infinite grid of a homogeneous medium. (b) Semi-infinite grid of a homogeneous medium with a matching PML. Scattered fields are present but are not explicitly shown.

It is easily shown that in the limit as $\alpha_{x1} \to \infty$ we obtain $u(t)\alpha_{x1}e^{-\alpha_{x1}t} = \delta(t)$, i.e., the delta function. We then find $[(1 - b_{x1})\delta(t) + u(t)b_{x2}\alpha_{x2}e^{-\alpha_{x2}t}] * (\partial H_z/\partial x)$ has the same form of (5) from [7], where for equality $(1 - b_{x1}) = 1/k_i$, $b_{x2}\alpha_{x2} = \sigma_i/k_i^2\varepsilon_0$ and $\alpha_{x2} = (\sigma_i/k_i\varepsilon_0) + (\alpha_i/\varepsilon_0)$. Note that $[b_{x1}, b_{x2}, \alpha_{x2}]$ represent three independent parameters of the CCO-PML while $[k_i, \sigma_i, \alpha_i]$ represent three independent parameters of (5) of [7].

V. 3-D Reflection Coefficient Derivation

The purpose of this section is to develop a method for calculating the reflection coefficient from a plane wave, in a general linear medium, incident onto the Nth-order CCO-PML for a given set of CCO-PML coefficients and a given PML cell thickness, T. The incident plane wave is taken to be a function of incident angle, including complex angles, frequency, and polarization (important for anisotropic media). The reflection coefficient calculation quantifies the scattered plane wave field, i.e., the error due to the PML. The motivation for this calculation is that any general electromagnetic field can be described by a linear superposition of both evanescent and propagating plane waves.

We begin by presenting the calculation of the properties of our incident plane wave [pictorially depicted in Fig. 1(a)]. We assume the wave is in an infinite homogeneous medium, i.e., without the PML. As in [10]–[12] we assume single frequency and plane wave fields. The incident wave has the following form:

$$\begin{aligned}e^{j\omega n\Delta t}e^{-j(k_x i_x\Delta x + k_y i_y\Delta y + k_z i_z\Delta z)} &= e^{j\omega n\Delta t} \\ &\times e^{-j(k\sin(\theta)\cos(\phi)i_x\Delta x + k\sin(\theta)\sin(\phi)i_y\Delta y + k\cos(\theta)i_z\Delta z)} \quad (9)\end{aligned}$$

where i_x, i_y, i_z are all integer indices (note: the indices i_x, i_y, i_z will now be replaced with the indices i, j, k. The $j = \sqrt{-1}$ term is also in the equations but the indices i, j, k always appear together so there should be no confusion.). Also we have $k_x = k\sin(\theta)\cos(\phi)$, $k_y = k\sin(\theta)\sin(\phi)$, and $k_z = k\cos(\theta)$.

The wave number k is the actual wave number in the FDTD grid for a given frequency and propagation angle. For example, the dispersion characteristics for the plane wave in an FDTD space of a homogeneous isotropic medium is described by the following:

$$\left[\bar{\varepsilon}\frac{2j\sin\frac{\omega\Delta t}{2}}{\Delta t}+\sigma\cos\frac{\omega\Delta t}{2}\right]\mu_0\frac{2j\sin\frac{\omega\Delta t}{2}}{\Delta t} = \left(\frac{2j\sin\frac{k\sin(\theta)\cos(\phi)\Delta x}{2}}{\Delta x}\right)^2+\left(\frac{2j\sin\frac{k\sin(\theta)\sin(\phi)\Delta y}{2}}{\Delta y}\right)^2 + \left(\frac{2j\sin\frac{k\cos(\theta)\Delta z}{2}}{\Delta z}\right)^2 \tag{10}$$

which allows us to solve for k for any given propagation angle and frequency. For anisotropic mediums, the dispersion relationships is not so simple but can be calculated. We will show how to solve for k for the mediums presented. Note: we treat the electrical polarization currents, J, in the following analysis. For ease of presentation, the magnetic polarization currents, M are set to zero. When they are present, they would be treated in the same way as we treat J. The spatial relationships for the fields, E_x and H_y, are

$$E_x|^{n,\omega}_{i+.5\pm1,j\pm1,k\pm1} = E_x|^{n,\omega}_{i+.5,j,k}e^{\mp jk_x\Delta x}e^{\mp jk_y\Delta y}e^{\mp jk_z\Delta z} \tag{11a}$$

$$H_y|^{n+.5,\omega}_{i+.5\pm1,j\pm1,k+.5\pm1} = H_y|^{n+.5,\omega}_{i+.5,j,k+.5}e^{\mp jk_x\Delta x}e^{\mp jk_y\Delta y}e^{\mp jk_z\Delta z}. \tag{11b}$$

The above examples are directly applicable to deriving the spatial relationships for E_y, E_z, H_y, H_z. We also assume the following time relationships for E_x, and H_y

$$E_x|^{n\pm1,\omega}_{i+.5,j,k} = E_x|^{n,\omega}_{i+.5,j,k}e^{\pm j\omega\Delta t} \tag{12a}$$

$$H_y|^{n+.5\pm1,\omega}_{i+.5,j,k+.5} = H_y|^{n+.5,\omega}_{i+.5,j,k+.5}e^{\pm j\omega\Delta t}. \tag{12b}$$

The above examples are directly applicable to deriving the time relationships for E_y, E_z, H_y, H_z. The following set of equations define plane wave propagation in our medium (note: we use the field variables E_{xi}, E_{yi}, E_{zi}, H_{xi}, H_{yi}, H_{zi} where the i is there simply to state that this is our incident field.)

$$\bar{\varepsilon}\frac{e^{j\omega\Delta t}-1}{\Delta t}E_{xi}|^{n,\omega}_{i+.5,j,k}+J_{xi}|^{n+.5,\omega}_{i+.5,j,k} = -\frac{1-e^{jk_z\Delta z}}{\Delta z}H_{yi}|^{n+.5,,\omega}_{i+.5,j,k+.5} + \frac{1-e^{jk_y\Delta y}}{\Delta y}H_{zi}|^{n+.5,\omega}_{i+.5,j+.5,k} \tag{13}$$

$$\bar{\varepsilon}\frac{e^{j\omega\Delta t}-1}{\Delta t}E_{yi}|^{n,\omega}_{i,j+.5,k}+J_{yi}|^{n+.5,\omega}_{i,j+.5,k} = \frac{1-e^{jk_z\Delta z}}{\Delta z}H_{xi}|^{n+.5,\omega}_{i,j+.5,k+.5} - \frac{1-e^{jk_x\Delta x}}{\Delta x}H_{zi}|^{n+.5,\omega}_{i+.5,j+.5,k} \tag{14}$$

$$\bar{\varepsilon}\frac{e^{j\omega\Delta t}-1}{\Delta t}E_{zi}|^{n,\omega}_{i,j,k+.5}+J_{zi}|^{n+.5,\omega}_{i,j,k+.5} = -\frac{1-e^{jk_y\Delta y}}{\Delta y}H_{xi}|^{n+.5,\omega}_{i,j+.5,k+.5} + \frac{1-e^{jk_x\Delta x}}{\Delta x}H_{yi}|^{n+.5,\omega}_{i+.5,j,k+.5} \tag{15}$$

$$\mu_0\frac{1-e^{-j\omega\Delta t}}{\Delta t}H_{xi}|^{n+.5,\omega}_{i,j+.5,k+.5} = \frac{e^{-jk_z\Delta z}-1}{\Delta z}E_{yi}|^{n,\omega}_{i,j+.5,k} - \frac{e^{-jk_y\Delta y}-1}{\Delta y}E_{zi}|^{n,\omega}_{i,j,k+.5} \tag{16}$$

$$\mu_0\frac{1-e^{-j\omega\Delta t}}{\Delta t}H_{yi}|^{n+.5,\omega}_{i+.5,j,k+.5} = -\frac{e^{-jk_z\Delta z}-1}{\Delta z}E_{xi}|^{n,\omega}_{i+.5,j,k} + \frac{1-e^{jk_x\Delta x}}{\Delta x}E_{zi}|^{n,\omega}_{i,j,k+.5} \tag{17}$$

$$\mu_0\frac{1-e^{-j\omega\Delta t}}{\Delta t}H_{zi}|^{n+.5,\omega}_{i+.5,j+.5,k} = \frac{e^{-jk_y\Delta y}-1}{\Delta y}E_{xi}|^{n,\omega}_{i+.5,j,k} - \frac{1-e^{jk_x\Delta x}}{\Delta x}E_{yi}|^{n,\omega}_{i,j+.5,k} \tag{18}$$

where $J_{xi}|^{n+.5,\omega}_{i+.5,j,k}$, $J_{yi}|^{n+.5,\omega}_{i,j+.5,k}$, and $J_{zi}|^{n+.5,\omega}_{i,j,k+.5}$ represent the polarization currents and are, in general, frequency dependent and complicated averages in time and space of the surrounding electric fields. For example $J_{xi}|^{n+.5,\omega}_{i+.5,j,k}$ can be expressed as

$$J_{xi}|^{n+.5,\omega}_{i+.5,j,k} = \sigma_{11}\overline{E_{xi}}|^{n,\omega}_{i+.5,j,k} + \sigma_{12}\overline{E_{yi}}|^{n,\omega}_{i,j+.5,k} + \sigma_{13}\overline{E_{zi}}|^{n,\omega}_{i,j,k+.5} \tag{19}$$

Where $\overline{E_{xi}}$, $\overline{E_{yi}}$, and $\overline{E_{zi}}$ are spatial averages to collocate the fields and σ_{11}, σ_{12} and σ_{13} are, in general, frequency dependent. Using the relationships that were used to derive 11–16, a form of the polarization current which will be used for a validation test in the numerical results section [18] is

$$J_{xi}|^{n+.5,\omega}_{(i+.5,j,k)} = \sigma_{11}\frac{e^{-jk_x\Delta x}+2+e^{jk_x\Delta x}}{4}E_{xi}|^{n,\omega}_{i+.5,j,k} + \sigma_{12}\frac{1+e^{jk_y\Delta y}}{2}\frac{e^{-jk_x\Delta x}+1}{2}E_{yi}|^{n,\omega}_{i,j+.5,k} + \sigma_{13}\frac{1+e^{jk_z\Delta z}}{2}\frac{e^{-jk_x\Delta x}+1}{2}E_{zi}|^{n,\omega}_{i,j,k+.5} \tag{20}$$

$$J_{yi}|^{n+.5,\omega}_{i,j+.5,k} = \sigma_{21}\frac{e^{-jk_y\Delta y}+1}{2}\frac{1+e^{jk_x\Delta x}}{2}E_{xi}|^{n,\omega}_{i+.5,j,k} + \sigma_{22}\frac{e^{-jk_y\Delta y}+2+e^{jk_y\Delta y}}{4}E_{yi}|^{n,\omega}_{i,j+.5,k} + \sigma_{23}\frac{1+e^{jk_z\Delta z}}{2}\frac{e^{-jk_y\Delta y}+1}{2}E_{zi}|^{n,\omega}_{i,j,k+.5} \tag{21}$$

$$J_{zi}|^{n+.5,\omega}_{i,j,k+.5} = \sigma_{31}\frac{e^{-jk_z\Delta z}+1}{2}\frac{1+e^{jk_x\Delta x}}{2}E_{xi}|^{n,\omega}_{i+.5,j,k} + \sigma_{32}\frac{1+e^{jk_y\Delta y}}{2}\frac{e^{-jk_z\Delta z}+1}{2}E_{yi}|^{n,\omega}_{i,j+.5,k} + \sigma_{33}\frac{e^{-jk_z\Delta z}+2+e^{jk_z\Delta z}}{4}E_{zi}|^{n,\omega}_{i,j,k+.5}. \tag{22}$$

Our medium could range from free space (J = 0) to a complicated linear magnetized plasma. We now use the system of equations in the following ways.

1) We solve for the wave number k (with constraints $Re\{k\} \geq 0$, $Im\{k\} \leq 0$) by setting the determinate of the above system to zero and iteratively solve for k until the equality is satisfied (note: anisotropic media generally have two solutions for k (with constraints $Re\{k\} \geq 0$, $Im\{k\} \leq 0$), for which we must choose one. This is done for each frequency, ω, and incident angle, θ and ϕ of interest.)
2) We will solve for the fields at timestep, $n = 0$, and spatial location, $i = 0, j = j_0, k = k_0$. This is an arbitrary choice since we are solving for the steady state field amplitudes. For isotropic media we set $E_{zi}|^{n=0,\omega}_{i=0,j_0,k_0+.5} = 1.0$ and $H_{zi}|^{n=+.5,\omega}_{i=.5,j_0+.5,k_0} = 0.0$ (note: both of these fields values are arbitrary but both must be assigned values to uniquely define our incident wave). We then can explicitly solve for the other field components of the system
   a) $E_{yi}|^{n=0,\omega}_{i=0,j_0+.5,k_0} = A_y e^{j\phi_y}$
   b) $E_{xi}|^{n=0,\omega}_{i=.5,j_0,k_0} = A_x e^{j\phi_x}$
   c) $H_{xi}|^{n=+.5,\omega}_{i=0,j_0+.5,k_0+.5}$ and $H_{yi}|^{n=+.5,\omega}_{i=.5,j_0,k_0+.5}$.

   For anisotropic media we set $E_{zi}|^{n=0,\omega}_{i=0,j_0,k_0+.5} = 1.0$ (note: this field value is arbitrary but must be assigned a value to uniquely define our incident wave). We then can explicitly solve for the other field components of the system
   a) $E_{yi}|^{n=0,\omega}_{i=0,j_0+.5,k_0} = A_y e^{j\phi_y}$
   b) $E_{xi}|^{n=0,\omega}_{i=.5,j_0,k_0} = A_x e^{j\phi_x}$
   c) $H_{xi}|^{n=+.5,\omega}_{i=0,j_0+.5,k_0+.5}$, $H_{yi}|^{n=+.5,\omega}_{i=.5,j_0,k_0+.5}$, and $H_{zi}|^{n=+.5,\omega}_{i=.5,j_0+.5,k_0}$.

We have now uniquely defined our incident wave. We will now construct the time harmonic equations for the space depicted pictorially in Fig. 1(b) which includes the PML. This space, Fig. 1(b), for any given incident wave, produces a scattered wave, and with this information a reflection coefficient can be calculated. We begin by defining the PML to begin at $i = 1$, while the medium that the PML is matching exists is at $i = 0$, and $i = .5$. We will specify the boundary conditions at $i = 0$ to be the incident plus the scattered wave fields. We will assume nonzero CCO-PML coefficients, i.e., for $i >= 1$, in only the $\hat{x}$ direction. The y and z dependence of the fields within the PML are well defined since Snell's Law requires the PML fields to share the same y and z phase variation as the incident wave. However, within the space, PML included, the x dependence of the fields cannot be explicitly specified since in the x direction we have reflections, decay, etc. Inserting the harmonic time and spatial relationships, excluding the x-dependent relationship, into the CCO-PML FDTD equations we get the following set of equations (note: we use the field variables E_{xt}, E_{yt}, E_{zt}, H_{xt}, H_{yt}, H_{zt} where the t is there simply to state that this is total field.)

$$\bar{\varepsilon}\frac{e^{j\omega\Delta t}-1}{\Delta t}E_{xt}|^{n,\omega}_{i+.5,j,k}+J_{xt}|^{n+.5,\omega}_{i+.5,j,k} = -\frac{1-e^{jk_z\Delta z}}{\Delta z}H_{yt}|^{n+.5,\omega}_{i+.5,j,k+.5} + \frac{1-e^{jk_y\Delta y}}{\Delta y}H_{zt}|^{n+.5,\omega}_{i+.5,j+.5,k} \tag{23}$$

$$\bar{\varepsilon}\frac{e^{j\omega\Delta t}-1}{\Delta t}E_{yt}|^{n,\omega}_{i,j+.5,k}+J_{yt}|^{n+.5,\omega}_{i,j+.5,k} = \frac{1-e^{jk_z\Delta z}}{\Delta z}H_{xt}|^{n+.5,\omega}_{i,j+.5,k+.5} - \gamma_{x(\omega,i)}\frac{H_{zt}|^{n+.5,\omega}_{i+.5,j+.5,k}-H_{zt}|^{n+.5,\omega}_{i-.5,j+.5,k}}{\Delta x} \tag{24}$$

$$\bar{\varepsilon}\frac{e^{j\omega\Delta t}-1}{\Delta t}E_{zt}|^{n,\omega}_{i,j,k+.5}+J_{zt}|^{n+.5,\omega}_{i,j,k+.5} = -\frac{1-e^{jk_y\Delta y}}{\Delta y}H_{xt}|^{n+.5,\omega}_{i,j+.5,k+.5} + \gamma_{x(\omega,i)}\frac{H_{yt}|^{n+.5,\omega}_{i+.5,j,k+.5}-H_{yt}|^{n+.5,\omega}_{i-.5,j,k+.5}}{\Delta x} \tag{25}$$

$$\mu_0\frac{1-e^{-j\omega\Delta t}}{\Delta t}H_{xt}|^{n+.5,\omega}_{i,j+.5,k+.5} = \frac{e^{-jk_z\Delta z}-1}{\Delta z}E_{yt}|^{n,\omega}_{i,j+.5,k} - \frac{e^{-jk_y\Delta y}-1}{\Delta y}E_{zt}|^{n,\omega}_{i,j,k+.5} \tag{26}$$

$$\mu_0\frac{1-e^{-j\omega\Delta t}}{\Delta t}H_{yt}|^{n+.5,\omega}_{i+.5,j,k+.5} = -\frac{e^{-jk_z\Delta z}-1}{\Delta z}E_{xt}|^{n,\omega}_{i+.5,j,k} + \gamma_{x(\omega,i+.5)}\frac{E_{zt}|^{n,\omega}_{i+1,j,k+.5}-E_{zt}|^{n,\omega}_{i,j,k+.5}}{\Delta x} \tag{27}$$

$$\mu_0\frac{1-e^{-j\omega\Delta t}}{\Delta t}H_{zt}|^{n+.5,\omega}_{i+.5,j+.5,k} = \frac{e^{-jk_y\Delta y}-1}{\Delta y}E_{xt}|^{n,\omega}_{i+.5,j,k} - \gamma_{x(\omega,i+.5)}\frac{E_{yt}|^{n,\omega}_{i+1,j+.5,k}-E_{yt}|^{n,\omega}_{i,j+.5,k}}{\Delta x} \tag{28}$$

$$J_{xt}|^{n+.5,\omega}_{(i+.5,j,k)} = \sigma_{11}\frac{\left(E_{xt}|^{n,\omega}_{i+1.5,j,k}+2E_{xt}|^{n,\omega}_{i+.5,j,k}+E_{xt}|^{n,\omega}_{i-.5,j,k}\right)}{4} + \sigma_{12}\frac{1+e^{jk_y\Delta y}}{2}\frac{\left(E_{yt}|^{n,\omega}_{i,j+.5,k}+E_{yt}|^{n,\omega}_{i+1,j+.5,k}\right)}{2} + \sigma_{13}\frac{1+e^{jk_z\Delta z}}{2}\frac{\left(E_{zt}|^{n,\omega}_{i,j,k+.5}+E_{zt}|^{n,\omega}_{i+1,j,k+.5}\right)}{2} \tag{29}$$

$$J_{yt}|^{n+.5,\omega}_{i,j+.5,k} = \sigma_{21}\frac{e^{-jk_y\Delta y}+1}{2}\frac{\left(E_{xt}|^{n,\omega}_{i+.5,j,k}+E_{xt}|^{n,\omega}_{i-.5,j,k}\right)}{2} + \sigma_{22}\frac{e^{-jk_y\Delta y}+2+e^{jk_y\Delta y}}{4}E_{yt}|^{n,\omega}_{i,j+.5,k} + \sigma_{23}\frac{1+e^{jk_z\Delta z}}{2}\frac{e^{-jk_y\Delta y}+1}{2}E_{zt}|^{n,\omega}_{i,j,k+.5} \tag{30}$$

$$J_{zt}|^{n+.5,\omega}_{i,j,k+.5} = \sigma_{31}\frac{e^{-jk_z\Delta z}+1}{2}\frac{\left(E_{xt}|^{n,\omega}_{i+.5,j,k}E_{xt}|^{n,\omega}_{i-.5,j,k}\right)}{2} + \sigma_{32}\frac{1+e^{jk_y\Delta y}}{2}\frac{e^{-jk_z\Delta z}+1}{2}E_{yt}|^{n,\omega}_{i,j+.5,k} + \sigma_{33}\frac{e^{-jk_z\Delta z}+2+e^{jk_z\Delta z}}{4}E_{zt}|^{n,\omega}_{i,j,k+.5} \tag{31}$$

where

$$\gamma_x(\omega,i)=1-\sum_{n=1}^{N}\frac{b_{xn}(i)}{2}\left(\frac{\left[1-e^{-\alpha_{xn}(i)\Delta t}\right]}{1-e^{-\alpha_{xn}(i)\Delta t}e^{-j\omega\Delta t}}+\frac{\left[-1+e^{-j\omega\Delta t}\right]\left[\frac{1-\alpha_{xn}(i)\Delta t e^{-\alpha_{xn}(i)\Delta t}-e^{-\alpha_{xn}(i)\Delta t}}{\alpha_{xn}(i)\Delta t}\right]}{1-e^{-\alpha_{xn}(i)\Delta t}e^{-j\omega\Delta t}}\right)-\sum_{n=1}^{N}\frac{b^*_{xn}(i)}{2}\left(\frac{\left[1-e^{-\alpha^*_{xn}(i)\Delta t}\right]}{1-e^{-\alpha^*_{xn}(i)\Delta t}e^{-j\omega\Delta t}}+\frac{\left[-1+e^{-j\omega\Delta t}\right]\left[\frac{1-\alpha^*_{xn}(i)\Delta t e^{-\alpha^*_{xn}(i)\Delta t}-e^{-\alpha^*_{xn}(i)\Delta t}}{\alpha^*_{xn}(i)\Delta t}\right]}{1-e^{-\alpha^*_{xn}(i)\Delta t}e^{-j\omega\Delta t}}\right) \quad (32)$$

and where, for example, $\gamma_x(\omega,i)((H_{zt}|^{n+.5,\omega}_{i+.5,j+.5,k}-H_{zt}|^{n+.5,\omega}_{i-.5,j+.5,k})/\Delta x)$ represents $(\partial H_{zt}/\partial x)-Re\{\sum_{n=1}^{N}u(t)b_{xn}\alpha_{xn}e^{-\alpha_{xn}t}\}*(\partial H_{zt}/\partial x)$, the x dependent CCO curl operation on H_{zt}. The terms

$$\left(\frac{\left[1-e^{-\alpha_{xn}(i)\Delta t}\right]}{1-e^{-\alpha_{xn}(i)\Delta t}e^{-j\omega\Delta t}}+\frac{\left[-1+e^{-j\omega\Delta t}\right]\left[\frac{1-\alpha_{xn}(i)\Delta t e^{-\alpha_{xn}(i)\Delta t}-e^{-\alpha_{xn}(i)\Delta t}}{\alpha_{xn}(i)\Delta t}\right]}{1-e^{-\alpha_{xn}(i)\Delta t}e^{-j\omega\Delta t}}\right) \quad (33)$$

in $\gamma_x(\omega,i)$ are derived using the piecewise linear recursive convolution technique (PLRC) whose difference equation is

$$\Psi|^n=\Psi|^{n-1}e^{-\alpha\Delta t}+F|^n\left(1-e^{-\alpha\Delta t}-\frac{1-e^{-\alpha\Delta t}-\alpha\Delta t e^{-\alpha\Delta t}}{\alpha\Delta t}\right)+F|^{n-1}\left(\frac{1-e^{-\alpha\Delta t}-\alpha\Delta t e^{-\alpha\Delta t}}{\alpha\Delta t}\right) \quad (34)$$

which represents $\Psi=u(t)\alpha e^{-\alpha t}*F$ (where F is any time domain function, e.g., $\partial H_{zt}/\partial x$. In our case, aside from different complex amplitude valued fields, the time domain function is $F=e^{-j\omega t}$, since we are assuming single frequency fields). The electric fields at the $i=T+1$ cell in Fig. 1(b) will be assumed to be zero, i.e $E_{zt}|^{n,\omega}_{i=T+1,j,k+.5}=E_{yt}|^{n,\omega}_{i=T+1,j+.5,k}=0$, since we will treat the outer boundary of the space as perfect electric conductor (PEC). We can now define the total electric field boundary conditions at $i=0$, $i=-.5$ (note: the $i=-.5$ boundary condition is only needed for the anisotropic medium presented in this paper), $j=j_0$, $k=k_0$ and at timestep, $n=0$, to be

$$E_{xt}|^{n=0,\omega}_{i=-.5,j_0,k_0}=E_{xi}|^{n=0,\omega}_{i=-.5,j_0,k_0}+E_{xs}|^{n=0,\omega}_{i=-.5,j_0,k_0}=A_x e^{j\phi_x}e^{jk_x\Delta x}+E_{xs}|^{n=0,\omega}_{i=-.5,j_0,k_0} \quad (35)$$

$$E_{yt}|^{n=0,\omega}_{i=0,j_0+.5,k_0}=E_{yi}|^{n=0,\omega}_{i=0,j_0+.5,k_0}+E_{ys}|^{n=0,\omega}_{i=0,j_0+.5,k_0}=A_y e^{j\phi_y}+E_{ys}|^{n=0,\omega}_{i=0,j_0+.5,k_0} \quad (36)$$

$$E_{zt}|^{n=0,\omega}_{i=0,j_0,k_0+.5}=E_{zi}|^{n=0,\omega}_{i=0,j_0,k_0+.5}+E_{zs}|^{n=0,\omega}_{i=0,j_0,k_0+.5}=1.0+E_{zs}|^{n=0,\omega}_{i=0,j_0,k_0+.5} \quad (37)$$

which represents the incident wave plus the scattered wave (E_{xs}, E_{yx}, E_{zs} represent the scattered fields due to the PML) at the boundary of the FDTD space. To close our system of equations, i.e., make them uniquely solvable, we need to specify the total electric fields on the boundary. We have already specified the incident fields. We can represent the scattered electric boundary fields, $E_{xs}|^{n=0,\omega}_{i=-.5,j_0,k_0}$, $E_{ys}|^{n=0,\omega}_{i=0,j_0+.5,k_0}$, $E_{zs}|^{n=0,\omega}_{i=0,j_0,k_0+.5}$, in terms of the scattered magnetic fields, $H_{xs}|^{n=+.5,\omega}_{i=0,j_0+.5,k_0+.5}$, $H_{ys}|^{n=+.5,\omega}_{i=.5,j_0,k_0+.5}$, $H_{zs}|^{n=+.5,\omega}_{i=.5,j_0+.5,k_0}$. We have

$$H_{xs}|^{n=+.5,\omega}_{i=0,j_0+.5,k_0+.5}=H_{xt}|^{n=+.5,\omega}_{i=0,j_0+.5,k_0+.5}-H_{xi}|^{n=+.5,\omega}_{i=0,j_0+.5,k_0+.5} \quad (38)$$

$$H_{ys}|^{n=+.5,\omega}_{i=.5,j_0,k_0+.5}=H_{yt}|^{n=+.5,\omega}_{i=.5,j_0,k_0+.5}-H_{yi}|^{n=+.5,\omega}_{i=.5,j_0,k_0+.5} \quad (39)$$

$$H_{zs}|^{n=+.5,\omega}_{i=.5,j_0+.5,k_0}=H_{zt}|^{n=+.5,\omega}_{i=.5,j_0+.5,k_0}-H_{zi}|^{n=+.5,\omega}_{i=.5,j_0+.5,k_0}. \quad (40)$$

By doing so we close our system since boundary conditions are now specified by our incident fields and the total magnetic fields just inside the boundary from which we can uniquely solve the system. For ease of presentation let

$$E_i|^{n=0,\omega}=\begin{pmatrix}E_{xi}|^{n=0,\omega}_{i=-.5,j_0,k_0}\\E_{yi}|^{n=0,\omega}_{i=0,j_0+.5,k_0}\\E_{zi}|^{n=0,\omega}_{i=0,j_0,k_0+.5}\end{pmatrix} \quad (41)$$

$$H_i|^{n=.5,\omega}=\begin{pmatrix}H_{xi}|^{n=+.5,\omega}_{i=0,j_0+.5,k_0+.5}\\H_{yi}|^{n=+.5,\omega}_{i=.5,j_0,k_0+.5}\\H_{zi}|^{n=+.5,\omega}_{i=.5,j_0+.5,k_0}\end{pmatrix} \quad (42)$$

where $E_s|^{n=0,\omega}$ and $H_s|^{n=.5,\omega}$ will have the same form as well. We now describe the procedure for specifying the scattered boundary electric fields by relating $E_s|^{n=0,\omega}$ to $H_s|^{n=.5,\omega}$. We do the following:

1) For the isotropic case, Snell's law requires that $k_x=-k_{xs}$, $k_y=k_{ys}$, $k_z=k_{zs}$, or simply the reflected wave number is preserved and the reflected angle equals the incident angle.
   a) We use (13)–(18), replacing the field variables $E_i|^{n=0,\omega}$, $H_i|^{n=.5,\omega}$ with $E_s|^{n=0,\omega}$, $H_s|^{n=.5,\omega}$ and replacing k_x, k_y, k_z with k_{xs}, k_{ys}, k_{zs} This give us a unique system of equations relating $E_s|^{n=0,\omega}$ to $H_s|^{n=.5,\omega}$.
2) The anisotropic case is more complicated. When reflected from the PML, the single mode incident wave, be it a right-hand elliptically polarized (RHEP) or left-hand elliptically polarized (LHEP) wave, can couple into both the LHEP and RHEP reflected modes [19]. Also, because this is an anisotropic medium, even though Snell's law is satisfied, the angle of incidence does not necessarily equal the angle of reflection. This is because the reflected wave number k is a function of propagation direction, θ and ϕ, and polarization.
   a) We require $H_s|^{n=.5,\omega}=H_{s1}|^{n=.5,\omega}+H_{s2}|^{n=.5,\omega}$ where $H_{s1}|^{n=.5,\omega}$ and $H_{s2}|^{n=.5,\omega}$ are the scattered RHEP and LHEP modes, respectively.
   b) For the scattered modes we enforce Snell's law $k_y=k_{ys1}=k_{ys2}$, $k_z=k_{zs2}=k_{zs1}$. This allows us to determine, k_{xs1}, and k_{xs2}. For k_{xs1} use (13)–(18), replacing k_x, k_y, k_z with k_{xs1},

k_{ys1}, k_{zs1}, and set the determinate of the system to zero. We solve for k_{xs1} with the constraints that $Re\{k_{xs1}\} \leq 0$, $Im\{k_{xs1}\} \geq 0$ and the polarization of the resultant wave is RHEP. We do the same for solving k_{xs2} with constraints $Re\{k_{xs2}\} \leq 0$, $Im\{k_{xs2}\} \geq 0$ and the polarization of the resultant wave is LHEP.

c) We use (13)–(18), replacing the field variables $E_i|^{n=0,\omega}$, $H_i|^{n=.5,\omega}$ with $E_{s1}|^{n=0,\omega}$, $H_{s1}|^{n=.5,\omega}$ and replacing k_x, k_y, k_z with k_{xs1}, k_{ys1}, k_{zs1} This system of equations relates $E_{s1}|^{n=0,\omega}$ to $H_{s1}|^{n=.5,\omega}$.

d) Again, using (13)–(18) we replace the field variables $E_i|^{n=0,\omega}$, $H_i|^{n=.5,\omega}$ with $E_{s2}|^{n=0,\omega}$, $H_{s2}|^{n=.5,\omega}$ and replacing k_x, k_y, k_z with k_{xs2}, k_{ys2}, k_{zs2}. This system of equations relates $E_{s2}|^{n=0,\omega}$ to $H_{s2}|^{n=.5,\omega}$.

e) We require $H_s|^{n=.5,\omega} = H_{s1}|^{n=.5,\omega} + H_{s2}|^{n=.5,\omega}$ and $E_s|^{n=0,\omega} = E_{s1}|^{n=0,\omega} + E_{s2}|^{n=0,\omega}$. We now have a unique system of equations relating $E_s|^{n=0,\omega}$ to $H_s|^{n=.5,\omega}$.

The total electric field boundary conditions are now fully specified. This information closes our system of equations and makes all unknowns solvable which we can calculate using matrix techniques. The field matrix vectors, E_{xt}, H_{yt}, H_{zt}, in our above system of matrix equations each contain $\mathrm{T}+1$ unknown variables, while field matrix vectors, H_{xt}, E_{yt}, E_{zt}, each contain T unknown variables. We can now solve for all fields in the space defined but moreover we now calculate three important quantities: $H_{xs}|^{n=+.5,\omega}_{i=0,j_0+.5,k_0+.5}$, $H_{ys}|^{n=+.5,\omega}_{i=.5,j_0,k_0+.5}$ and $H_{zs}|^{n=+.5,\omega}_{i=.5,j=j_0+.5,k_0}$. We define the normalized error between the two systems as

$$\|R(\omega,\theta,\phi)\|_2 = \sqrt{\frac{|H_s|^{n=.5,\omega}|^2}{|H_i|^{n=.5,\omega}|^2}}. \tag{43}$$

This is simply the normalized Euclidean norm of the scattered magnetic field due to the PML, i.e., the magnitude of the reflection coefficient. For ease of presentation we will refer to $\|R(\omega,\theta,\phi)\|_2$ as the reflection coefficient due to the PML for a given frequency and angle of incidence. We can, therefore, adjust the CCO-PML coefficients, $b_{xn}(i)$ and $\alpha_{xn}(i)$ until $\|R(\omega,\theta,\phi)\|_2$ is minimized over the frequencies and incident angles of interest. Fig. 2 displays a particular $\|R(\omega,\theta,\phi)\|_2$ versus frequency, for a particular incident angle. We can improve $\|R(\omega,\theta,\phi)\|_2$. by setting a band of minimum reflection, $0 < \omega < \omega_c$. We would require $\|R(\omega,\theta,\phi)\|_2 < \alpha_c$ for $0 < \omega < \omega_c$. Or we could require $\|R(\omega,\theta,\phi)\|_2 < \alpha_c$ for $0 < \omega < \omega_c$, which is the average reflection coefficient. Another requirement would be to have $\|R(\omega,\theta,\phi)\|_2 < \alpha_p = 1.0$ for $\omega > \omega_c$. This condition forces the boundary condition to be stable over all frequencies. We would minimize α_c for a given ω_c by iteratively adjusting the CCO-PML coefficients, given an initial starting value for the CCO-PML coefficients, until α_c reaches a minimum. In most cases we would minimize over a range of incident angles as well. This is the procedure used in this paper for improving the PML to match particular mediums, the results of which are presented in the numerical results section.

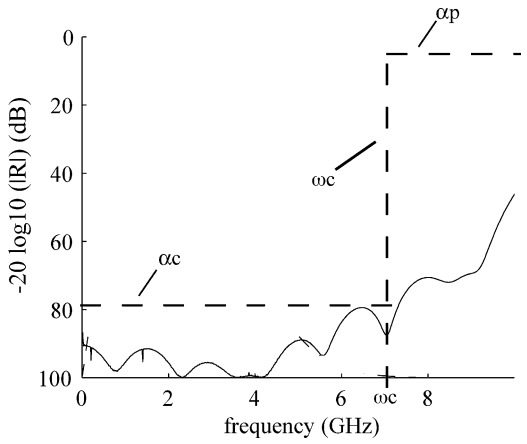

Fig. 2. Typical reflection coefficient with design constraints.

VI. Numerical Tests

To validate our method, we calculate the reflection coefficient from time domain simulations of the space in Fig. 1(b). We do this by selecting a portion of the space as illustrated in Fig. 3(a). This portion is an FDTD grid, displayed as an orthographic projection representation in Fig. 3(b)-(d). The grid is a $3\times3\times(T+1)$ cell space where the center front cell represents the $(i=0, j=j_0, k=k_0)$ cell, our reference cell used to derive the analytical reflection coefficient from Section V. Note: we could have used any $M\times N\times(T+1)$ cell space, where M, $N>2$. In order for the fields within the FDTD grid to represent an incident plane wave being scattered from the PML, we must properly specify the grid's surface boundary fields over time, whose locations are indicated by the bold black line segments. From Section V our method for calculating the reflection coefficient also allowed us to calculate ALL fields within the PML, and the entire space of Fig. 1(b) for that matter, as a function of frequency, incident angle, and the input incident fields. This means we know $E_{xt}|^{n=0,\omega}_{i-.5,j_0,k_0}$, $E_{yt}|^{n=0,\omega}_{i,j_0+.5,k_0}$, and $E_{zt}|^{n=0,\omega}_{i,j_0,k_0+.5}$ for $i=0$: $T+1$. For a given angle of incidence, we apply the plane wave relations in the y and z directions

$$\widetilde{E_{xt}}|^{\omega}_{i-.5,j_0+m,k_0+p} = E_{xt}|^{n=0,\omega}_{i-.5,j_0,k_0} e^{-j(k_y m\Delta y + k_z p\Delta z)} \tag{44}$$

$$\widetilde{E_{yt}}|^{\omega}_{i,j_0+.5+m,k_0+p} = E_{yt}|^{n=0,\omega}_{i,j_0+.5,k_0} e^{-j(k_y m\Delta y + k_z p\Delta z)} \tag{45}$$

$$\widetilde{E_{zt}}|^{\omega}_{i,j_0+m,k_0+.5+p} = E_{zt}|^{n=0,\omega}_{i,j_0,k_0+.5} e^{-j(k_y m\Delta y + k_z p\Delta z)} \tag{46}$$

to calculate the grid surface boundary fields as a function of frequency (where m and p are integers whose allowed values correspond to all fields located on the grid surface). (Note: the $\sim$ symbol above the field variables associates these fields with the $3\times3\times(T+1)$ cell space.) This is enough information to do the simulations. Our general procedure for calculating the reflection coefficient using the time domain simulation is

1) We multiply grid surface boundary fields by the input spectrum of the incident wave, $S(\omega)$, and compute the in-

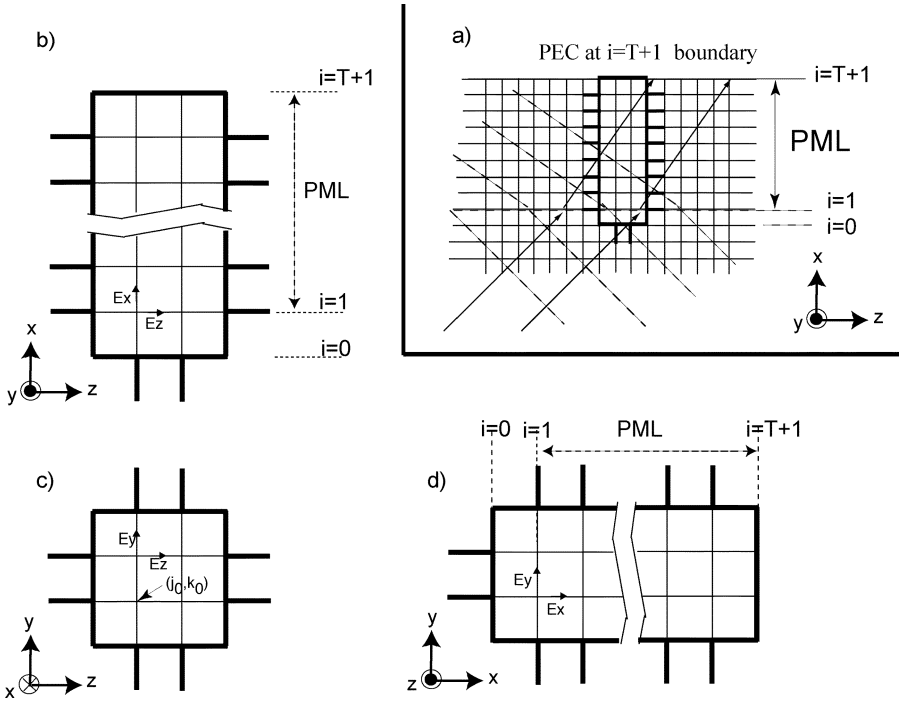

Fig. 3. Orthographic projection representation of the $3 \times 3 \times (T+1)$ cell FDTD space used to calculate the PML reflection coefficient in the time domain numerical experiments.

TABLE I
CCO-PML COEFFICIENT PROFILE, PROFILE A

i	$b_{x1}(i)$	$e^{\alpha_{x1}(i)\Delta t}$	i	$b_{x1}(i)$	$e^{\alpha_{x1}(i)\Delta t}$
1.0	1.0	0.9997	6.0	1.0	0.8012
1.5	1.0	0.9984	6.5	1.0	0.7421
2.0	1.0	0.9953	7.0	1.0	0.6730
2.5	1.0	0.9897	7.5	1.0	0.5941
3.0	1.0	0.9807	8.0	1.0	0.5062
3.5	1.0	0.9674	8.5	1.0	0.4115
4.0	1.0	0.9487	9.0	1.0	0.3142
4.5	1.0	0.9237	9.5	1.0	0.2203
5.0	1.0	0.8914	10.0	1.0	0.1379
5.5	1.0	0.8508	10.5	1.0	0.0741

verse FFT these fields to obtain the time domain boundary fields as follows:

$$\widetilde{E_{xt}}|^n_{i-.5,j_0+m,k_0+p} = \mathrm{FFT}^{-1}\left(\widetilde{E_{xt}}|^{\omega}_{i-.5,j_0+m,k_0+p}\right) = \mathrm{FFT}^{-1}\left(E_{xt}|^{n=0,\omega}_{i-.5,j_0,k_0} e^{-j(k_y m\Delta y + k_z p\Delta z)} S(\omega)\right) \quad (47)$$

$$\widetilde{E_{yt}}|^n_{i,j_0+.5+m,k_0+p} = \mathrm{FFT}^{-1}\left(\widetilde{E_{yt}}|^{\omega}_{i,j_0+.5+m,k_0+p}\right) = \mathrm{FFT}^{-1}\left(E_{yt}|^{n=0,\omega}_{i,j_0+.5,k_0} e^{-j(k_y m\Delta y + k_z p\Delta z)} S(\omega)\right) \quad (48)$$

$$\widetilde{E_{zt}}|^n_{i,j_0+m,k_0+.5+p} = \mathrm{FFT}^{-1}\left(\widetilde{E_{zt}}|^{\omega}_{i,j_0+m,k_0+.5+p}\right) = \mathrm{FFT}^{-1}\left(E_{zt}|^{n=0,\omega}_{i,j_0,k_0+.5} e^{-j(k_y m\Delta y + k_z p\Delta z)} S(\omega)\right). \quad (49)$$

2) We run the FDTD equations within the space coupled with the grid surface boundary fields while saving $\widetilde{H_{xt}}|^n_{i=0,j_0+.5,k_0+.5}$, $\widetilde{H_{yt}}|^{n+.5}_{i=+.5,j_0,k_0+.5}$ and $\widetilde{H_{zt}}|^{n+.5}_{i=+.5,j_0+.5,k_0}$ over time.
3) We compute the FFT of these field values and divide by the input spectrum to normalize the fields as follows:

$$\widehat{H_{xt}}|^{\omega}_{i=0,j_0+5,k_0+.5} = \frac{\mathrm{FFT}\left(\widetilde{H_{xt}}|^n_{i=0,j_0+.5,k_0+.5}\right)}{S(\omega)} \quad (50)$$

$$\widehat{H_{yt}}|^{\omega}_{i=+.5,j_0,k_0+.5} = \frac{\mathrm{FFT}\left(\widetilde{H_{yt}}|^n_{i=+.5,j_0,k_0+.5}\right)}{S(\omega)} \quad (51)$$

$$\widehat{H_{zt}}|^{\omega}_{i=+.5,j_0+.5,k_0} = \frac{\mathrm{FFT}\left(\widetilde{H_{zt}}|^n_{i=+.5,j_0+.5,k_0}\right)}{S(\omega)}. \quad (52)$$

4) We have $\widehat{H_s}|^{\omega} = \widehat{H_t}|^{\omega} H_i|^{n=.5,\omega}$, where we define $\widehat{H_t}|^{\omega}$ and $\widehat{H_s}|^{\omega}$ in the same manner as $H_i|^{n=.5,\omega}$ was defined in (42). We calculate the reflection coefficient with the following:

$$\left\|\widehat{R}(\omega,\theta,\phi)\right\|_2 = \sqrt{\frac{|\widehat{H_s}|^{\omega}|^2}{|H_i|^{n=.5,\omega}|^2}}. \quad (53)$$

This time domain method (TD method) for calculating the reflection coefficient is equivalent to the frequency domain derivation (FD method) from Section V. Mathematically, they must yield the same results over the spectral energy range of $S(\omega)$ because both methods originate from the same difference equations. Any differences are due to numerical error.

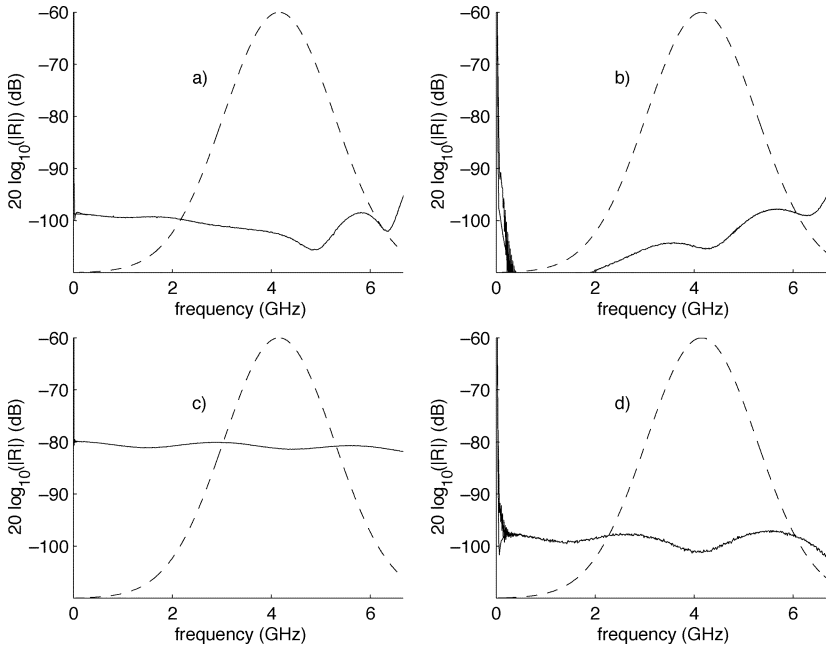

Fig. 4. Refection coefficient for the FD and TD methods ($S(\omega)$ also plotted) for various angles of incidence (free space). (a) Profile A, ($\theta = \pi/3$, $\phi = \pi/10$). (b) Profile B, ($\theta = \pi/3$, $\phi = \pi/10$). (c) Profile A, ($\theta = \pi/2$, $\phi = \pi/2.9$). (d) Profile B, ($\theta = \pi/2$, $\phi = \pi/2.9$).

We present three numerical experiments. Each numerical experiment involves calculating the reflection coefficient of a plane wave incident onto the PML at various angles of incidence or modes. For all numerical experiments the incident wave time domain input pulse at $\widetilde{E_{zi}}|_{i=0,j_0,k_0+.5}^{n}$ is a modulated gaussian with a full-width half-maximum of $45\Delta t$ and a modulation radial frequency of $2\pi/12.5\Delta t$. We display a CCO-PML coefficient profile, Profile A, shown in Table I, where in all numerical tests we apply Profile A. Profile A is an order, $N = 1$, CCO-PML and has only real coefficients. In all the numerical tests we also apply an optimized profile. Note: Profile A is the initial profile given to the optimizer for every optimized profile presented in the numerical experiments. We use gradient methods which will yield a local minimum, not necessarily a global minimum. We optimize $\overline{||R(\omega,\theta,\phi)||_2}$ for our frequency range of interest.

A. Free Space Plane Waves Incident Onto the PML

Our first experiment compares the calculation of the reflection coefficient for a free space plane wave incident on the PML for both the FD and TD methods. This is done for two different incident angles, ($\theta = \pi/3$, $\phi = \pi/10$) and ($\theta = \pi/2$, $\phi = \pi/2.9$). The cell size of our space is, $\Delta x = \Delta y = \Delta z$ =0.01 m. The TD method was run for 4000 timesteps. We ran the optimization scheme from Section V, using Profile A as the input profile, optimizing an order $N = 1$ profile with complex coefficients. The resulting locally minimized profile we call "Profile B." The reflection coefficients using Profile A for the two different angles of incidence are respectively shown in Fig. 4(a) and (c). The reflection coefficients using Profile B for the two different angles of incidence are respectively shown in Fig. 4(b) and (d). In each case, the FD and TD methods are identical for the spectral energy range of $S(\omega)$ (also plotted), except in Fig. 4(b) and (d) where there is some fuzz at the lowest frequencies. This is typically due to the TD method not running for enough timesteps and therefore not properly converging to zero fields. For the incidence angle ($\theta = \pi/3$, $\phi = \pi/10$), the reflection coefficients for Profile A and Profile B are similar. For the incidence angle ($\theta = \pi/2$, $\phi = \pi/2.9$) the reflection coefficient for Profile B is about 18 dB better on the average. At the lowest frequencies, the reflection coefficients for Profile B have a poorer response. The maximum frequency plotted in Fig. 4 equates to 4.5 cells per free space wavelength.

B. Magnetoplasma Plane Waves Incident Onto the PML

Our second experiment compares the calculation of the reflection coefficient for a right-hand elliptically polarized plane wave in an anisotropic magnetoplasma incident on the PML for both the FD and TD methods. To model our plasma we apply the method of Lee and Kalluri [18]. Their method can be derived into the anisotropic tensor, $\vec{J} = \sigma\vec{E}$ whose form is (29)–(31). This was done for two different incident angles, ($\theta = \pi/3$, $\phi = \pi/10$) and ($\theta = \pi/2$, ϕ =0). The cell size of our space is, $\Delta x = \Delta y = \Delta z = 10$ m. The parameters of the magnetoplasma are the ambient magnetic field, $\vec{B}_0 = 1 \times 10^{-5}\hat{a_x}$, the electron density $N_e = 1 \times 10^{11}$, and the collision frequency $\nu = 5 \times 10^6$. The TD method was run for 8000 timesteps. We ran the optimization scheme from Section V, using Profile A as the input profile. Our optimized profile is an order $N = 2$ profile with complex coefficients which we call "Profile C." The reflection coefficients using Profile A for the two different angles of incidence are respectively shown in Fig. 5(a) and (c). The reflection coefficients using Profile C for the two different angles of incidence are respectively shown in Fig. 5(b) and (d). In each case, the FD and TD methods are identical for the spectral energy range of $S(\omega)$ (also plotted), except for some fuzz at the lower and higher frequencies due to not running the TD method long enough. Fig. 5(a) shows a peak between 1.8 and

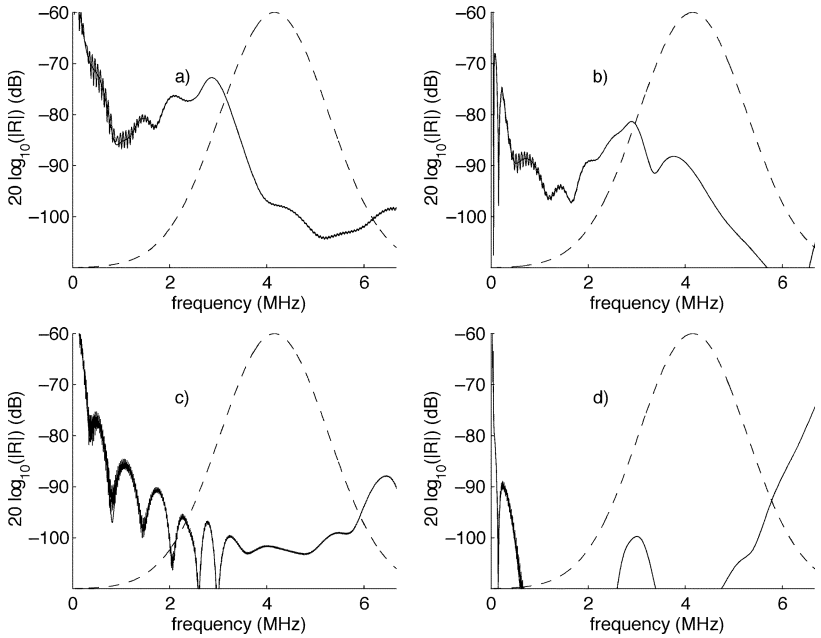

Fig. 5. Refection coefficient for the FD and TD methods ($S(\omega)$ also plotted) for various angles of incidence (magnetoplasma). (a) Profile A, ($\theta = \pi/3$, $\phi = \pi/10$). (b) Profile C, ($\theta = \pi/3$, $\phi = \pi/10$). (c) Profile A, ($\theta = \pi/2$, $\phi = 0$). (d) Profile C, ($\theta = \pi/2$, $\phi = 0$).

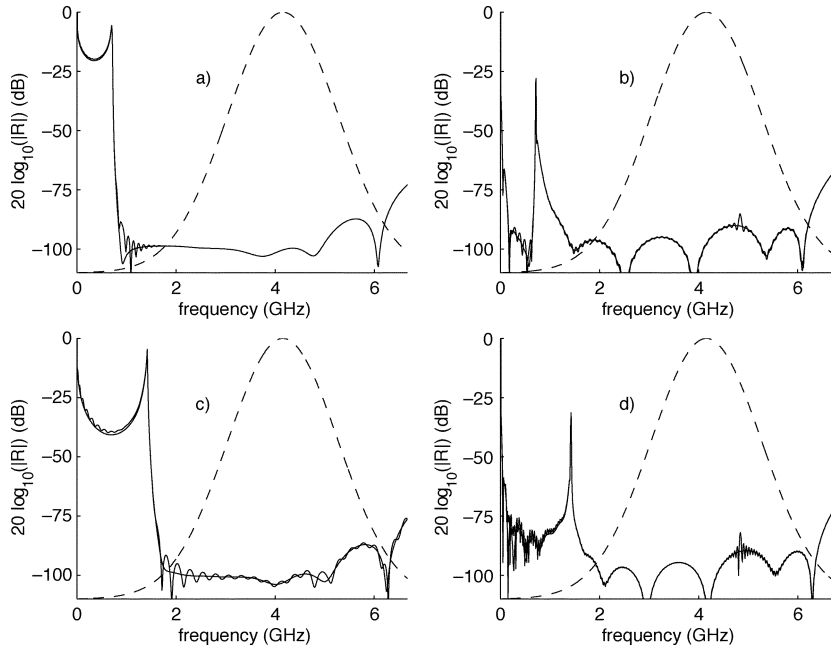

Fig. 6. Refection coefficient for the FD and TD methods ($S(\omega)$ also plotted) for various incident modes (free space waveguide). (a) Profile A, $n = 1$ mode. (b) Profile D, $n = 1$ mode. (c) Profile A, $n = 2$ mode. (d) Profile D, $n = 2$ mode.

3.8 MHz. We see that in Fig. 5(b) Profile C is able to reduce this peak. We had originally tried optimizing an order $N = 1$ profile, but that resulting profile was not able to remove the peak. The lower frequency responses are also better for Profile B as well. The maximum frequency plotted in Fig. 5 equates to 4.5 cells per free space wavelength.

C. Waveguide Modes Incident Onto the PML

Our final numerical experiment examines the performance of the optimized PML for TMz free space waveguide modes, propagating and evanescent. The dispersion relationship for the modes are

$$\varepsilon_0\mu_0\left(\frac{2j\sin\frac{\omega\Delta t}{2}}{\Delta t}\right)^2 = \left(\frac{2j\sin\frac{k\sin(\theta)\cos(\phi)\Delta x}{2}}{\Delta x}\right)^2 + \left(\frac{2j\sin\frac{k\sin(\theta)\sin(\phi)\Delta y}{2}}{\Delta y}\right)^2 + \left(\frac{2j\sin\frac{k\cos(\theta)\Delta z}{2}}{\Delta z}\right)^2 \tag{54}$$

$$k\sin(\theta)\sin(\phi)\Delta y = \frac{n\pi}{N_{\text{cells}}+1} \tag{55}$$

where $\theta = (\pi/2)$. The wave number, k, and the complex angle ϕ are obtained from the two equations above. N_{cells} is the cellular width of the waveguide and n is the mode number. Our FDTD space has $\Delta x = \Delta y = \Delta z = .01$ m. We calculated solutions for modes $n = 1, 2$. Again we apply the TD method since we still have an incident plane wave, albeit evanescent or propagating. The TD method was run for 6000 timesteps. We ran the optimization scheme from Section V, using Profile A as the input profile. Our optimized profile is an order $N = 1$ profile with complex coefficients which we call "Profile D." The reflection coefficients using Profile A for the two different modes are respectively shown in Fig. 6(a) and (c). The reflection coefficients using Profile D for the two different modes are respectively shown in Fig. 6(b) and (d). In each case, the FD and TD methods are identical for the spectral energy range of $S(\omega)$ (also plotted), except for some fuzz due to not running the TD method long enough. For both modes, the evanescent regions of the reflection coefficient are much improved using Profile D. The reflection coefficients are similar within the propagating regions for the two profiles. The maximum frequency plotted in Fig. 6 equates to 4.5 cells per free space wavelength.

VII. Summary

We described a new time-domain representation, the Nth order CCO-PML, which proves to be simple to implement for any linear medium. A frequency domain method for analytically examining the performance of the PML for linear media was developed. Time domain experiments were performed to validate the frequency domain method. The experiments also validated the range of mediums the CCO-PML is able to match. Optimization techniques were employed to demonstrate the capability of minimizing the error due to the PML.

References

[1] J. P. Berenger, "A perfectly matched layer for the absorption of electromagnetic waves," *J. Comput. Phys.*, vol. 114, pp. 185–200, 1994.

[2] W. C. Chew and W. H. Weedon, "A 3-D perfectly matched medium form modified Maxwell's equations with stretched coordinates," *Microw. Opt. Technol. Lett.*, vol. 7, no. 13, pp. 599–604, Sept. 1994.

[3] S. G. Gedney, "An anisotropic perfectly matched layer-absorbing medium for the truncation of FDTD lattices," *IEEE Trans. Antennas Propagat.*, vol. 44, pp. 1630–1639, Dec. 1996.

[4] J. Fang, "Generalized perfectly matched layer—an extension of Berenger's perfectly matched layer boundary condition," *IEEE Microwave Guided Wave Lett.*, vol. 5, pp. 451–453, Dec. 1995.

[5] F. L. Teixeira *et al.*, "A general approach to extend Berenger's absorbing boundary condition to anisotropic and dispersive media," *IEEE Trans. Antennas Propagat.*, vol. 46, pp. 1386–1387, Sept. 1998.

[6] M. W. Chevalier, "A perfectly-matched-layer boundary condition for use in FDTD modeling of pulse propagation in the earth-ionosphere waveguide," presented at the URSI/Radio Science Conf., Boulder, CO, 1999.

[7] J. A. Roden and S. D. Gedney, "Convolutional PML (CPML): an efficient FDTD implementation of the CFS-PML for arbitrary media," *Microwave Opt. Technol. Lett.*, vol. 27, no. 5, pp. 334–339, 2000.

[8] S. D. Gedney, G. Liu, J. A. Roden, and A. M. Zhu, "Perfectly matched layer media with CFS for an unconditionally stable ADI-FDTD method," *Proc. IEEE APS*, vol. 49, no. 11, pp. 1554–1559, 2001.

[9] O. Ramadan and A. Y. Oztoprak, "DSP techniques for the implementation of perfectly matched layer for truncating FDTD domains," *Electron. Lett.*, vol. 38, no. 5, pp. 211–212, 2002.

[10] W. C. Chew and J. M. Jin, "Perfectly matched layer in the discretized medium. An analysis and optimization," *Electromagn.*, vol. 16, no. 4, pp. 325–340, July 1996.

[11] J. Fang and Z. Wu, "Closed form expression of numerical reflection coefficient at PML interfaces and optimization of PML performance," *IEEE Microwave Guided Wave Lett.*, vol. 6, pp. 332–334, Sept. 1996.

[12] J. P. Berenger, "Evanescent waves in PML's: origin of the numerical reflection in wave-structure interaction problems," *Proc. IEEE APS*, vol. 47, pp. 1497–1503, Oct. 1999.

[13] ——, "Numerical reflections from FDTD-PML's: a comparison of the split PML with the unsplit and CFSPMLs," *Proc. IEEE APS*, vol. 50, pp. 258–265, Mar. 2002.

[14] ——, "Application of the CFSPML to the absorption of evanescent waves in waveguides," *IEEE Microwave Wireless Components Lett.*, vol. 12, pp. 218–220, June 2002.

[15] D. Kelley and R. Luebbers, "Piecewise linear recursive convolution for dispersive media using FDTD," *IEEE Trans. Antennas Propagat.*, vol. 44, pp. 792–798, June 1996.

[16] K. Kunz and R. Luebbers, *The Finite Difference Time Domain Method for Electromagnetics*. Boca Raton, FL: CRC, 1993.

[17] A. Taflove, Ed., *Finite Difference Time Domain Methods for Electrodynamic Analyzes*. New York: Artech House, May 1995.

[18] J. H. Lee and D. K. Kalluri, "Three-dimensional FDTD simulation of electromagnetic wave transformation in a dynamic inhomogeneous magnetized plasma," *IEEE Trans. Antennas Propagat.*, vol. 47, pp. 1146–1151, Sept. 1999.

[19] J. A. Ratcliffe, *The Magneto-Ionic Theory and Its Applications to the Ionosphere*. Cambridge, U.K.: Cambridge Univ. Press, 1959.

[20] J. A. Bittencourt, Ed., *Fundamentals of Plasma Physics*, Brazil: Sao Jose dos Campos, 1995.

[21] J. A. Stratton, *Electromagnetic Theory*. New York: McGraw-Hill, 1941.

Michael W. Chevalier was born in Washington, DC, on July 28, 1972. He received the B.S.E.E. degree from the University of New Hamphire, Durham, NH, in 1996 and the M.S.E.E. degree from Pennsylvania State University, State College, PA, in 1997. He is currently working toward the Ph.D. degree at Stanford University under Prof. Inan.

His research interests include numerical techniques for extremely low frequency (ELF) electromagnetic propagation in plasmas and within the earth-ionosphere waveguide. He is also working on measuring conductivity changes due to electron precipitation in the Auroral D-region of the ionosphere using very low frequency (VLF) remote sensing techniques.

Umran S. Inan (S'76–M'77–SM'99) was born in Turkey on December 28, 1950. He received the B.S. and M.S. degrees in electrical engineering from the Middle East Technical University, Ankara, Turkey, in 1972 and 1973, respectively, and the Ph.D. degree in electrical engineering from Stanford University, Stanford, CT, in 1977.

He is currently a Professor of electrical engineering at Stanford University, where he serves as Director of the Space, Telecommunications, and Radioscience (STAR) Laboratory. He actively conducts research in electromagnetic waves in plasmas, lightning discharges, ionospheric physics, and very low frequency remote sensing. He has served as the Ph.D. thesis adviser for 19 students.

Dr. Inan is a Member of Tau Beta Pi, Sigma Xi, the American Geophysical Union, and the Electromagnetics Academy. He received the 1998 Stanford University Tau Beta Pi Award for Excellence in Undergraduate Teaching. He serves as the current Chair of the United States National Committee of the International Union of Radio Science (URSI) and the International Chair of Commission H (Waves in Plasmas) of URSI.